

UNIVERSITY of CALIFORNIA  
SANTA CRUZ

**THERMAL EVOLUTION OF URANUS AND NEPTUNE WITH  
CONDENSATION-INHIBITED CONVECTION**

A thesis submitted in partial satisfaction of the  
requirements for the degree of

BACHELOR OF SCIENCE

in

ASTROPHYSICS

by

**Robert Schroder**

December 2020

Copyright © by

Robert Schroder

2020

## **Abstract**

Thermal Evolution of Uranus and Neptune with Condensation-inhibited Convection

by

Robert Schroder

This will be the last section written, once we have finished our results and conclusion.

# Contents

<b>List of Figures</b>	<b>v</b>
<b>List of Tables</b>	<b>vi</b>
<b>1 Introduction</b>	<b>1</b>
1.1 Condensation in Hydrogen Dominated Atmospheres . . . . .	3
<b>2 Model</b>	<b>6</b>
2.1 Three-layer Model with Dry Adiabat . . . . .	6
2.2 Inclusion of Moist Adiabat Within Outer Envelope . . . . .	8
2.3 Temperature Jump Across the Water Condensation Zone . . . . .	11
2.4 Energy Conservation and Thermal Evolution of Model . . . . .	13
<b>3 Results</b>	<b>14</b>
3.1 Condensation-inhibited Convection . . . . .	14
3.2 Formation of Radiative Zone . . . . .	15
3.3 Thermal Evolution of Uranus and Neptune . . . . .	16
<b>4 Discussion and Conclusions</b>	<b>25</b>

# List of Figures

2.1	A Standard Interior Structure Model . . . . .	7
2.2	Interior Structure for Moist Adiabat . . . . .	9
2.3	A Standard Interior Structure Model . . . . .	11
3.1	Inhibition of convection on Uranus . . . . .	18
3.2	Impact of Radiative Layer on T10 . . . . .	19
3.3	Formation of Radiative Zone . . . . .	20
3.4	Thermal Evolution Curves for Uranus - Adiabat Comparisons . . . . .	21
3.5	Thermal Evolution Curves for Uranus - Water Vapor Concentration Comparisons . . . . .	22
3.6	Thermal Evolution Curves for Neptune - Water Vapor Concentration Comparisons . . . . .	23
3.7	Thermal Evolution Curves for Uranus - Radius . . . . .	24
3.8	Thermal Evolution Curves for Neptune - Radius . . . . .	24

## List of Tables

# 1

## Introduction

Planets coalesce from matter contained in their parent star's protoplanetary disk.

As planets accrete material from the disk, it heats up, giving the planet a so-called 'hot start'. After accretion is complete, the planet will begin to cool over time. It will be helpful to define what we mean by temperature. There are several temperatures that describe a planet's atmosphere. The effective temperature,  $T_{\text{eff}}$ , is defined as the total flux integrated over all frequencies of a black body of the same shape and same distance as the planet (Seager, 2010).

$$\pi \int_0^{\infty} B(T, \nu) d\nu = \sigma_R T^4 \quad (1.1)$$

yielding,

$$T_{\text{eff}} = \left( \frac{F}{\sigma_R} \right)^{\frac{1}{4}} \quad (1.2)$$

The equilibrium temperature,  $T_{\text{eq}}$ , is the temperature the planet would have if it were in thermal equilibrium with its parent star. This occurs when the planet has radiated away its latent heat of formation, and the only remaining source of energy is from its star. This

temperature is defined as:

$$T_{\text{eq}}^4 = \frac{F(1 - A_B)}{r^2 4\pi \sigma_B} \quad (1.3)$$

where  $r$  is the distance from the star in AU,  $A_B$  is the bond albedo, and  $F$  is the solar flux. Finally, the intrinsic temperature,  $T_{\text{int}}$ , the temperature that defines the flux from the planet's interior and is defined by the relation:

$$T_{\text{eff}}^4 = T_{\text{eq}}^4 + T_{\text{int}}^4 \quad (1.4)$$

In 1965, Frank Low measured Jupiter's intrinsic temperature (Low, 1966). To explain this observation, theorists set out to expand on prior work (Demarcus, 1958) on the theory of interior structure of solar system gas and ice giants (Hubbard, 1968; Smoluchowski, 1967; Hubbard, 1977, 1978; M. Podolak, 1991). Models have assumed that the interior of giant planets are convective, meaning that heat within the planet's interior is transferred by the movement of fluids. More specifically, warmer, less dense material will rise; while cooler, more dense material will sink due to the influence of gravity. In 1968, Hubbard showed that a convective interior would allow Jupiter's observed flux to be transported to the surface adiabatically. This analysis motivated the inclusion of adiabatic interiors in contemporary interior structure models for gas and ice giants.

At the present time, most of the giant planets in our solar system: Saturn, Jupiter, and Neptune, all have an intrinsic flux. Uranus is the exception (Pearl & Conrath, 1991). Measurements of Uranus's effective temperature are consistent with a planet that has no intrinsic flux, a planet in thermal equilibrium with the Sun, cooler than its more distant neighbor, Neptune, a planet with similar mass and composition.

While thermal evolution models do currently reproduce  $T_{\text{eff}}$  for Jupiter and Nep-

tune at 4.6 Gyr (Graboske et al., 1975; Fortney et al., 2011), they do not reproduce  $T_{\text{eff}}$  for Saturn and Uranus. Models for Saturn predict a cooler planet; however, plausible explanations have been offered to explain its current, warmer  $T_{\text{eff}}$ . Among them, the rain-out of helium (Fortney & Hubbard, 2003; Mankovich & Fortney, 2019), or double-diffusive convection (Leconte & Chabrier, 2013).

Meanwhile, for Uranus, the models have predicted a warmer effective temperature at present time (Fortney et al., 2011; M. Podolak, 1991; W.B. Hubbard, 1995; L. Scheibe, 2019). There have been various attempts to explain Uranus' cool temperature. Early investigations posited that a stratified interior, stable against convection, would allow heat to be trapped deep within the the interior (M. Podolak, 1991). If the interior were stable against convection, some other means of energy transport must be responsible for transporting heat from the interior to the surface. Later work investigated possible mechanisms for energy transport other than dry,adiabatic convection. [NEED TO WORK ON THIS] The formation of stable condensation zones (Friedson & Gonzales, 2017), (Leconte et al., 2017), and (Guillot, 1995), and thermal boundary layers (Nettelmann et al., 2016), that could inhibit convection. It was speculated that the presence of these thermal boundary layers, or condensation zones, could trap heat deep within the interior, allowing the envelope above to cool more rapidly, thereby lowering the planet's effective temperature.

## 1.1 Condensation in Hydrogen Dominated Atmospheres

Up to now, we have discussed convection, but we haven't explicitly called it dry convection. When we speak of dry convection, we are not taking into consideration the condensation of molecular species in the atmosphere. On Earth, the atmosphere undergoes

moist convection. As a parcel of air is lifted, it cools until it gets cold enough that water vapor condenses out, releasing latent heat of condensation which boosts convection. This release of latent heat alters the temperature-pressure profile, which now follows a moist adiabat. In addition to the temperature gradient, there may also be a gradient in mean molecular weight. On Earth, moist air is lighter than dry air. For example, H<sub>2</sub>O vapor (molecular mass = 18 g/mol), the primary condensate in Earth's atmosphere is lighter (not by much) than the background air which is composed primarily of N<sub>2</sub> (molecular mass = 28 g/mol). When H<sub>2</sub>O vapor abundance exceeds the saturation vapor pressure, the vapor condenses out of the atmosphere, resulting in a small vertical gradient in mean molecular weight. In Earth's atmosphere, this small gradient does not impose a significant barrier to convection. By contrast, in hydrogen dominated atmospheres such as Neptune and Uranus, the background gas is much lighter than the condensates. In this hydrogen-rich environment, when H<sub>2</sub>O condenses out of the atmosphere, a strong vertical gradient in mean molecular weight can be established, resulting in a negative buoyancy for the convecting parcel of gas. This can create a situation where the zone in which water condenses is stable against convection (Guillot, 1995), (Friedson & Gonzales, 2017), (Leconte et al., 2017). Thus far, we have been discussing H<sub>2</sub>O as the only condensate. However, other condensates such as NH<sub>3</sub> and CH<sub>4</sub> may impact convection as well. In this study, we consider H<sub>2</sub>O as the primary condensate as it likely has the largest impact. The reason for this is that if its abundance is supercritical, then it results in a larger superadiabicity (larger temperature gradient) than would be provided by either NH<sub>3</sub> or CH<sub>4</sub> (Guillot, 1995). Consideration of other condensates is planned for future work.

The work done by (Guillot, 1995), (Friedson & Gonzales, 2017), and (Leconte et al.,

2017) examined under what conditions stable condensation zones would form. In this paper, we apply the same physical mechanisms for the formation of stable water condensation zones. However, we expand on this by placing the formation of these stable, radiative layers in the context of a more complete model of interior structure for solar system ice giants. Furthermore, we investigate how these stable layers impact the cooling of the planets over time. In chapter 2, we give a brief description of conventional, dry-convective interior structure models and how our moist-convective model differs. We present our results in Chapter 3, describing where and when stable water condensation zones form, how they impact cooling within the interior, their impact thermal evolution, and their impact on heat flow at present time. In Chapter 4, we discuss our conclusions and offer suggestions for further work.

# 2

# Model

## 2.1 Three-layer Model with Dry Adiabat

We begin our description of the physics of our interior structure model by assuming spherical symmetry and conservation of mass:

$$\frac{dm}{dr} = 4\pi r^2 \rho \quad (2.1)$$

where  $dm$  is the mass contained within a sphere of radius  $r + dr$ , and  $\rho(r)$  is the density.

Hydrostatic equilibrium is also assumed and described by:

$$\frac{dP}{dr} = -\frac{Gm\rho}{r^2} \quad (2.2)$$

where  $P$  is the pressure and  $G$  is the gravitational constant.

We employ a three-layer interior structure, seen schematically in Figure 2.1. At the center of the planet is a core made of rock and ice. Moving outward, the inner envelope is  $H_2O$  dominated, with uniform concentrations of H, He, and  $H_2O$ . The outer envelope,

below 1 bars, contains trace amounts of H<sub>2</sub>O, but is mostly comprised of H and He. To accommodate the incredibly high temperatures and pressures experienced deep in the interior of giant planets, We use the MAZEVET EOS as our H-He equation of state (S. Mazevet & Potekhin, 2019). For metals, we use MH13SCVH EOS (Y. Miguel & Fayon, 2018). [How much more should I go into this?]

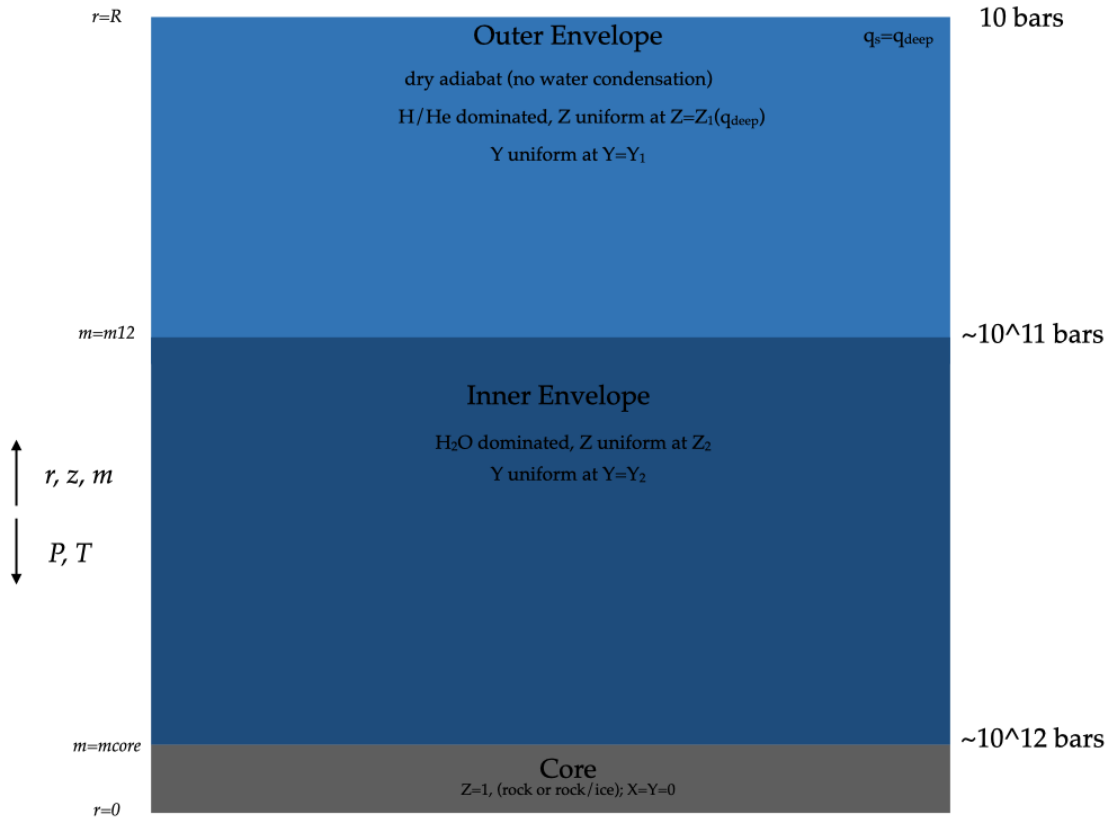


**Figure 2.1:** The structure for a fully convective, dry adiabatic interior. In this model, the inner and outer envelopes are assumed to be well mixed, fully convective, and following a dry adiabat. The core is composed of rock and ice. The inner envelope is water dominated, with uniform concentrations of hydrogen, helium, and water; whereas, the outer envelope is hydrogen and helium dominated, with trace amounts of water. The 'atmosphere' exists above 10 bars.

Historically, interior structure models have assumed that the interiors are com-

posed of compressible gases that are statically unstable and fully convective. In a dry-convective model such as this, a parcel of gas rises as its temperature increases while its pressure remains constant. This process happens without the addition or loss of heat from the parcel, a process referred to as adiabatic. Furthermore, while there may be a critical concentration for a condensable species, this dry model does not allow for condensation. The temperature-pressure profile follows a dry adiabat gradient (R. Kippenhahn, 2012), given by:

$$\nabla_{\text{ad}} = \left( \frac{\partial \ln T}{\partial \ln P} \right)_s \quad (2.3)$$

Finally, beyond the outer envelope is the atmosphere. When modeling the thermal evolution of gas and ice giants, it has long been recognized that model atmospheres constitute an outer boundary condition for interior structure models, providing key inputs that impact cooling times for interior structure models. Our work considered both (Graboske et al., 1975) and (Fortney et al., 2011) model atmospheres. In this paper, our results will utilize the Fortney 2011 model atmospheres.

## 2.2 Inclusion of Moist Adiabat Within Outer Envelope

Our interior structure model modifies the structure described in Section 2.1 by adding a moist adiabatic layer to the outer envelope, which under favorable conditions, allows for the condensation of  $H_2O$ . We define the moist adiabat as follows (Robinson, 2016):

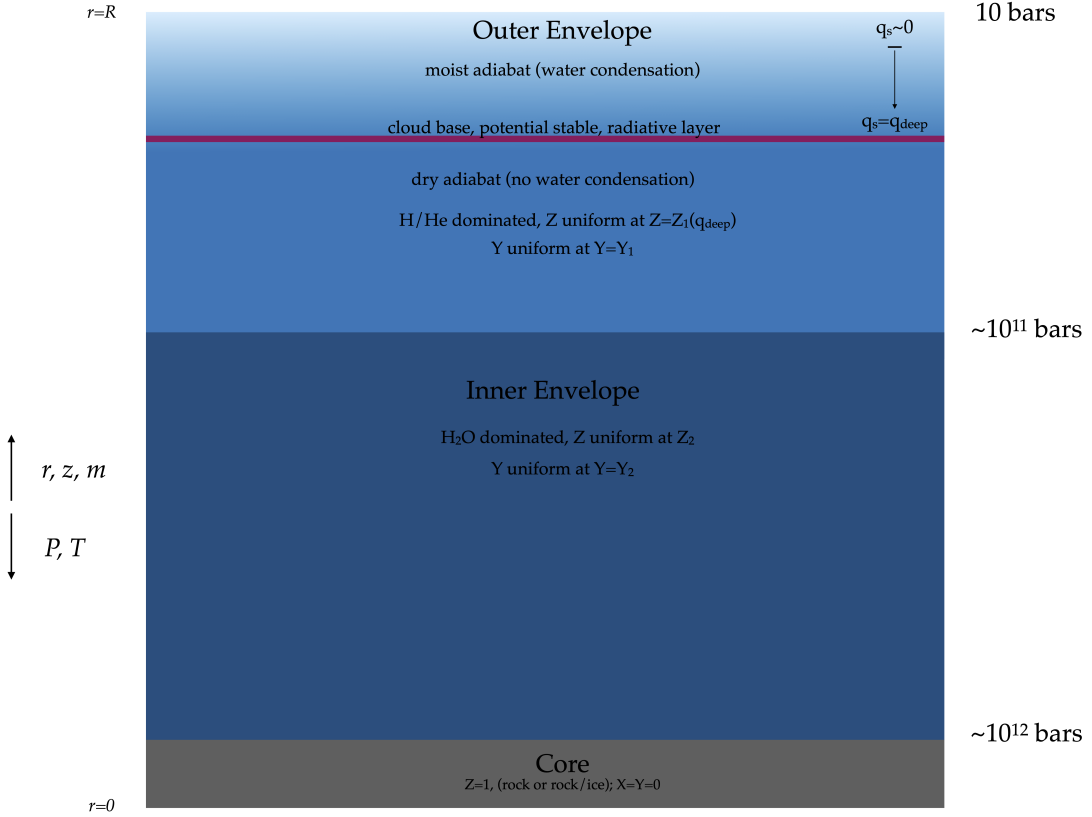


**Figure 2.2:** The structure for moist adiabatic interior, allowing for condensation-inhibited convection. In this model, a stable water condensation zone may form. The pressure and temperature at the base of the condensation zone is set by the condition that  $x_{\text{vap}}$  has reached the deep value  $x_{\text{vap}}^{\text{deep}}$ . Below the condensation zone, the temperature and pressure follow a dry adiabat.

$$\nabla_{\text{moist}} = \left( 1 + \frac{\frac{x_{\text{vap}} L}{R_{\text{gas}} T}}{\nabla_{\text{ad}} + \frac{L^2}{R_{\text{gas}}^2 T^2}} \right) \quad (2.4)$$

where,

$$\frac{dT}{dP} = \frac{T}{P} \nabla_{\text{moist}} \quad (2.5)$$

and the gradient of the water vapor mole fraction (Robinson, 2016) is given by,

$$\frac{dx_{\text{vap}}}{dP} = \frac{x_{\text{vap}} L}{R_{\text{gas}} T^2} \frac{dT}{dP} - \frac{x_{\text{vap}}}{P} \quad (2.6)$$

Gases condense at sufficiently low temperatures or high pressures. Condensation of a gas is characterized by its saturation vapor pressure, which derives from the Clausius-Clapeyron equation (Lavega, 2011). The saturation vapor pressure,  $P_{\text{sat}}$ , is given by:

$$P_{\text{sat}}(T) = P_{\text{sat}}(T_0) e^{-\frac{L+C_p T_0}{R_{\text{gas}}} \left(\frac{1}{T} - \frac{1}{T_0}\right) - \frac{C_p}{R_{\text{gas}}} \ln \frac{T}{T_0}} \quad (2.7)$$

where  $T_0 = 273.16K$ , and  $R_{\text{gas}}$  is the gas constant for the condensable species. When the partial pressure of a gas,  $P_{\text{gas}}$ , is less than  $P_{\text{sat}}$ , the parcel of gas is 'unsaturated'. When  $P_{\text{gas}} = P_{\text{sat}}$ , the gas is 'saturated'. And, when  $P_{\text{gas}} > P_{\text{sat}}$ , the parcel is 'supersaturated'. Every condensable species has its own saturation vapor pressure.

If condensation occurs, our model assumes that it may be stable against convection if a fast rain-out occurs such that the vertical gradient in mean molecular weight is large enough to counteract the positive buoyancy of the parcel of gas (Leconte et al., 2017) (Friedson & Gonzales, 2017). In this scenario, condensation-inhibited convection occurs when  $\alpha$  is negative, where  $\alpha$  (Friedson & Gonzales, 2017) is given by:

$$\alpha = 1 + \xi(q_s L / R_W T_0) \quad (2.8)$$

where  $R_{\text{vap}}$  is the gas constant for the vapor (water),  $T_0$  is the local temperature,  $L$  is the latent heat of vaporization for water,  $q_s$  is the saturation specific humidity, and  $\xi$  is given by  $\xi = \frac{1}{\epsilon} - 1$ , where  $\epsilon$  is the ratio of the molecular weight of vapor to the mean molecular weight of dry atmosphere. When  $\alpha$  is negative, the vertical gradient in molecular weight results in a stabilizing effect, overwhelming the effects due to latent heat release.

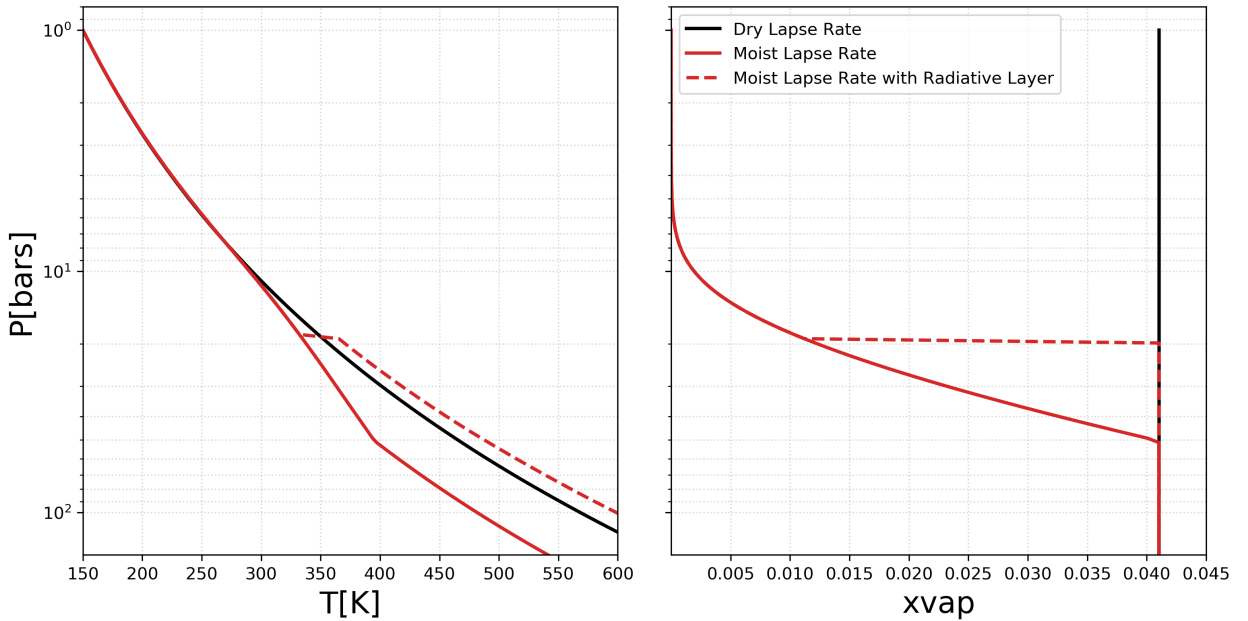


**Figure 2.3:** The solid red line is the moist adiabatic lapse rate. The solid black line is the dry lapse rate. The dashed red line is a moist lapse rate with the addition of a stable radiative layer (water condensation zone). The simple moist lapse rate is cooler at depth than either of the other two lapse rates. The presence of a stable radiative layer results in a warmer interior. These lapse rates assume  $q_{\text{deep}} = 0.25$  and  $T_1 = 150K$ , which is during the period when the onset of condensation-inhibited convection occurs.

### 2.3 Temperature Jump Across the Water Condensation Zone

Our model treats the water condensation zone (thin, stable, radiative layer) as a discontinuous increase in temperature. This, thin, stable, radiative layer has a temperature profile that is governed by:

$$T(P) = T_{\text{top}} + \int_{P_{\text{top}}}^{P_{\text{base}}} \left( \frac{dT}{dP} \right)_{\text{rad}} dP \quad (2.9)$$

with  $P_{\text{top}}$  and  $T_{\text{top}}$  denote the pressure and temperature at the top of the stable water condensation zone, and  $P_{\text{base}}$  represents the bottom of the zone. The integrand in Eqn. 2.9 is the radiative temperature gradient (Leconte et al., 2017), defined as:

$$\left(\frac{dT}{dP}\right)_{\text{rad}} = \frac{T}{P} \nabla_{\text{rad}} = \frac{T}{P} \times \frac{3}{16} \frac{\kappa_R P}{g} \frac{T_{\text{int}}^4}{T^4} \quad (2.10)$$

where  $T$  and  $P$  are the local temperature and pressure.  $T_{\text{int}}$  is the intrinsic temperature. The radiative temperature gradient across the water condensation zone is nearly constant, so that Eqn. 2.9 simplifies to:

$$T_{\text{base}} \equiv T(P + \Delta P) = T_{\text{top}} + \left(\frac{dT}{dP}\right)_{\text{rad}} \Delta P \quad (2.11)$$

where  $\Delta P$  is the extent of the pressure-space of the water condensation zone (radiative layer), given by:

$$\Delta P \equiv P_{\text{base}} - P_{\text{top}} = \frac{P_{\text{sat}}(T_{\text{base}})}{x_{\text{vap}}^{\text{deep}}} - P_{\text{top}}. \quad (2.12)$$

Within the condensation zone, the vapor mole fraction,  $x_{\text{vap}}$  is equal to the saturated vapor mole fraction:

$$x_{\text{vap}}(P, T) = x_{\text{vap}}^{\text{sat}}(P, T) = \frac{P_{\text{sat}}(T)}{P}, \quad P < P_{\text{base}}. \quad (2.13)$$

The base of the condensation zone is set by the condition that  $x_{\text{vap}}$  has reached the deep value  $x_{\text{vap}}^{\text{deep}}$ .

$$x_{\text{vap}}^{\text{sat}}(P_{\text{base}}, T_{\text{base}}) = \frac{P_{\text{sat}}(T_{\text{base}})}{P_{\text{base}}} = x_{\text{vap}}^{\text{deep}} \quad (2.14)$$

Below the water condensation zone, the region is subsaturated and hence no condensation occurs. Temperatures below the water condensation zone are obtained by integrating the dry adiabat  $\nabla_{\text{ad}}$ :

$$T(P > P_{\text{base}}) = T_{\text{base}} + \int_{P_{\text{base}}}^P \left(\frac{dT}{dP}\right)_{\text{ad}} dP \quad (2.15)$$

## 2.4 Energy Conservation and Thermal Evolution of Model

We borrow from conservation of energy and stellar structure and evolution to determine the timestep needed to evolve our model (R. Kippenhahn, 2012). We begin with the planets' intrinsic luminosity, defined as:

[not happy with this section at all.]

$$L_{\text{int}} = 4\pi R^2 \sigma_{\text{SB}} T_{\text{int}}^4 \quad (2.16)$$

And, the first law of thermodynamics states:

$$dQ = du + Pdv \quad (2.17)$$

where  $dQ$  is the heat added per unit mass,  $u$  is the internal energy per unit mass, and  $v = \frac{1}{\rho}$  per unit mass. So, for the heat per unit mass shell, we may write:

$$dQ = (\epsilon - \frac{dL}{dm})dt \quad (2.18)$$

Substituting our equation for the first law of thermodynamics, we arrive at:

$$\frac{\partial L}{\partial m} = \epsilon - \frac{\partial u}{\partial t} + \frac{P}{\rho^2} \frac{\partial \rho}{\partial t} \quad (2.19)$$

Here, we are not dealing with any nuclear reactions, so  $\epsilon = 0$ , giving us:

$$\frac{\partial L}{\partial m} = \frac{\partial u}{\partial t} + \frac{P}{\rho^2} \frac{\partial \rho}{\partial t} \quad (2.20)$$

# 3

# Results

## 3.1 Condensation-inhibited Convection

We began by looking at if and when condensation-inhibited convection would occur. We ran static models for a variety of  $T_{10}$ 's, the planet's temperature at 10 bars. The output of these static simulations are plotted in Figure 3.1. We ran our model with three different values of  $q_{\text{deep}}$ . The goal was to determine for each deep water concentration, at what pressures and temperatures, condensation-inhibited convection occurs. We find that for  $q_{\text{deep}} = 0.05$ , no condensation-inhibited convection occurred. In other words,  $\alpha$  (Eqn. 2.8) never takes on negative values with this concentration of water vapor, hence the condition for stability is never met. However, for larger values of  $q_{\text{deep}}$ , we find that  $\alpha$  does take on negative values (see rows 2 and 3 in Figure 3.1). The shaded regions of the plots indicate the pressure-space over which  $\alpha$  is negative. We show  $\alpha$  with respect to pressure, vapor mole fraction, and temperature. Note: the top of the shaded region in each plot indicates where the base of the condensation zone forms. [not sure if i should go into the

issue of the remainder of the shaded region having no physical meaning]. Looking at these plots, for  $q_{\text{deep}} = 0.15$  and  $q_{\text{deep}} = 0.25$ , we can see that condensation inhibited convection sets in at approximately  $T_{10} = 335K$ . Note: The  $T_{10}$  at which the onset of condensation occurs is dependent on the resolution of the simulation. As such, these plots are meant to show the likelihood of condensation-inhibited convection rather than the exact moment or specific deep water concentration for which it occurs. [I'm not very happy with the results section so far]

### 3.2 Formation of Radiative Zone

The plots in Figure 3.3 show the lapse rate (first column), and the change in the vapor mole fraction for  $H_2O$  (second column), for three different values of  $q_{\text{deep}}$ , 0.05, 0.15, and 0.25, for rows 1 through 3, respectively. In the first row, we can see that for early  $T_{10}$ 's, there is no onset of condensation, and the lapse rate follows a dry adiabat. For later  $T_{10}$ 's, there is a visible kink in the lapse rate which indicates the onset of condensation, at which point the lapse rate has a shallower slope. For the larger values of  $q_{\text{deep}}$ , where  $\alpha$  takes on negative values, we see the onset of condensation-inhibited convection and the establishment of a radiative zone. In the plots, the water condensation zones are represented by the horizontal discontinuities moving from left to right. As the planet cools, these radiative zones descend deeper into the planet's interior. When the radiative zones are established, the interior below the zone warms. Looking at Figure 3.2, we have overlayed the lapse rate for  $q_{\text{deep}} = 0.25$  (exhibiting stable water condensation zones) over the lapse rate for  $q_{\text{deep}} = 0.05$  (no stable zones). From this plot, one can see that the presence of a radiative zone creates a temperature jump such that a given  $T_{10}$  appears to look like an earlier  $T_{10}$ . In

other words, in the presence of radiative zones, the interior appears as warm as an interior described by an earlier  $T_{10}$ . [ugh. gotta be a better way to describe this]

Looking at the adjacent  $x_{\text{vap}}$  plots, we can see that  $x_{\text{vap}}$  follows its saturated value. At the bottom of the radiative zone, the vapor mole fraction equals its deep water value, which sets the conditions for the creation of the base of the condensation zone.

### 3.3 Thermal Evolution of Uranus and Neptune

We simulated the thermal evolution of Uranus and Neptune using a variety of variety of input parameters. In Figure 3.4, we display the results of evolutionary tracks that considered separately the evolution of a dry adiabat, a moist adiabat with condensation but no stable radiative zone, and a moist adiabat with condensation containing stable radiative zones. For all of these evolutionary tracks, we assumed  $q_{\text{deep}} = 0.25$ . Looking at these evolutionary tracks, the coolest scenario at present time, is a moist adiabat that is never stable against convection. The moist adiabat that is stable against convection has the warmest outcome at present time. In Figure 3.5 and Figure 3.6, we consider the impact of different deep water concentrations on the thermal evolution of Uranus and Neptune, respectively. As the planets cool, their radiative zones descend deeper into the interior, as we saw in Figure 3.3. This feature is also noticeable in the thermal evolution plots. Looking at  $T_{\text{eff}}$  at  $7 \times 10^7$  Gyr, the onset of condensation-inhibited convection occurs, resulting in a discontinuous temperature drop. The same behavior is seen in the  $T_{10}$  plot, however, by this time the radiative zone has descended deeper, later in time at around  $7 \times 10^8$  Gyr. Larger  $q_{\text{deep}}$ 's result in warmer Uranus and Neptune at present time. We also look at the impact of  $q_{\text{deep}}$  on the evolution of planetary radius and find that larger values of  $q_{\text{deep}}$  tend

to converge more closely toward the presently observed radius for both Uranus and Neptune in these simulations. [needs more work]

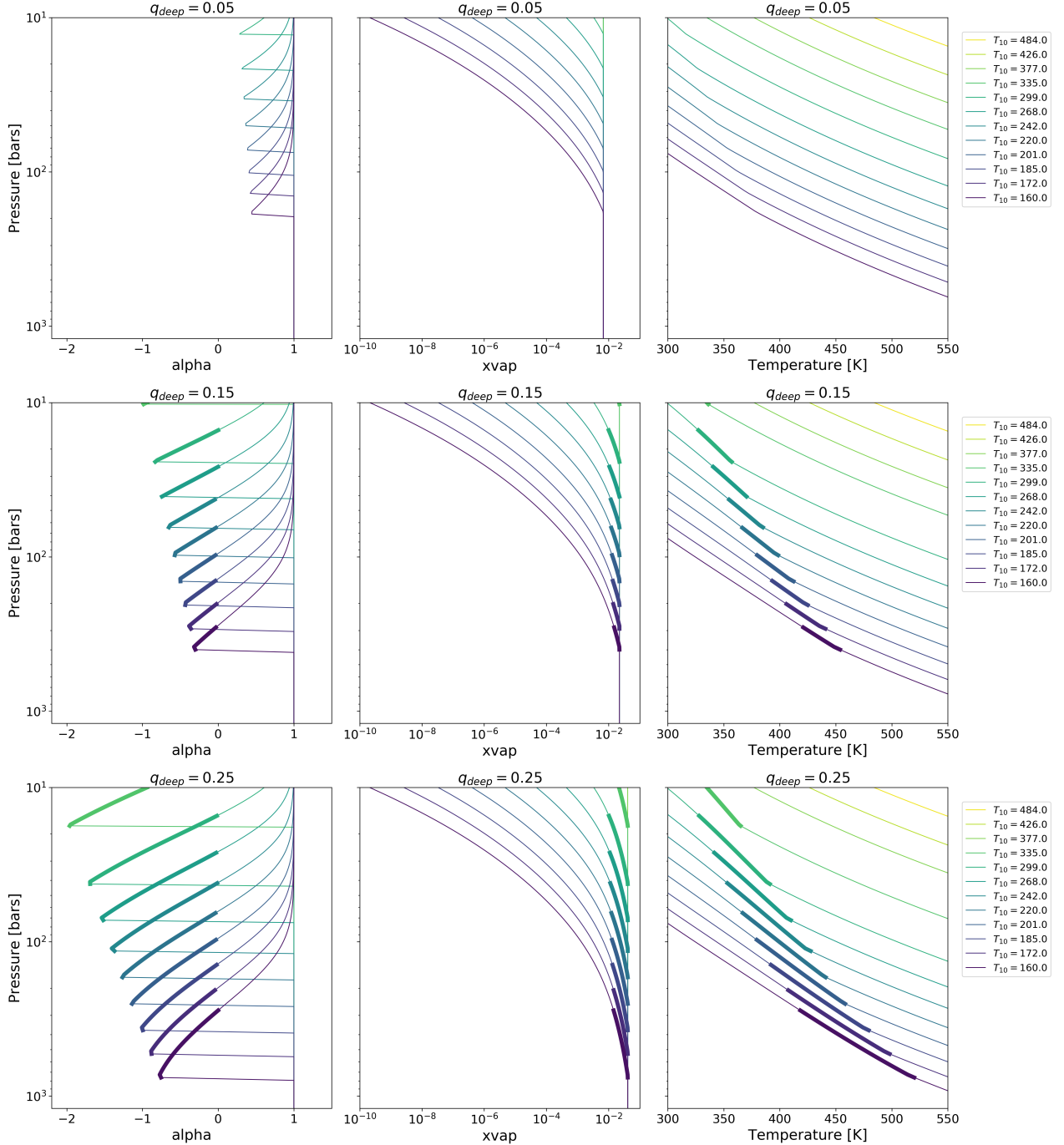


**Figure 3.1:** Each row represents a different value for  $q_{\text{deep}}$ . For the top row,  $q_{\text{deep}} = 0.05$ , for which no stable condensation zone forms. For the middle row,  $q_{\text{deep}} = 0.15$ , and for the third row  $q_{\text{deep}} = 0.25$ . For these concentrations, stable condensation zones can form. The shaded regions of the plots indicate zones where  $\alpha$  is negative, or where stable zones can form.

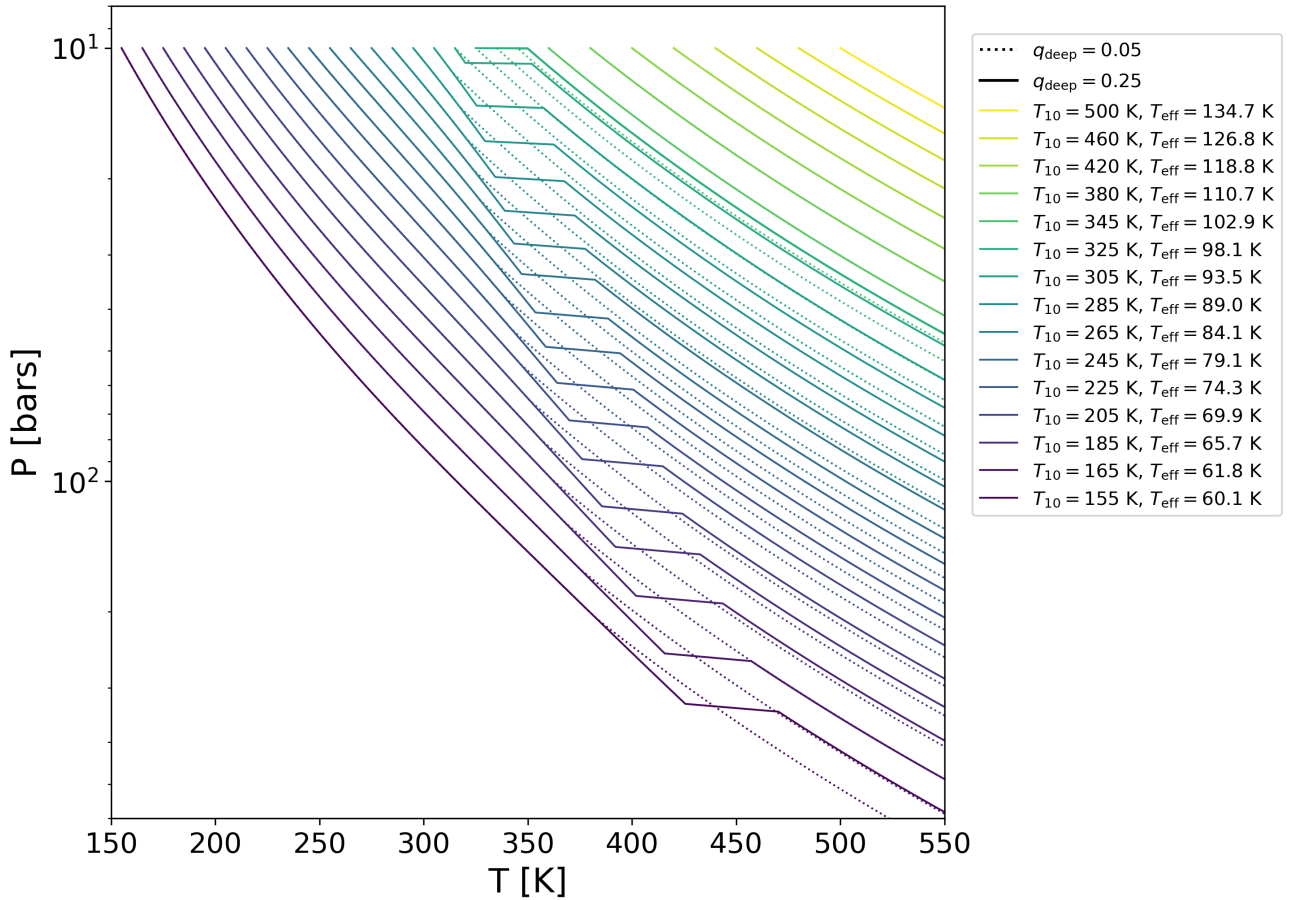


**Figure 3.2:** The solid lines represent the lapse rate for  $q_{\text{deep}} = 0.25$ , and the dashed lines for  $q_{\text{deep}} = 0.05$ . Looking at recent  $T_{10}$ 's, the lapse interior temperature for  $q_{\text{deep}} = 0.25$  jumps to an earlier  $t_{10}$ . The radiative layer traps heat, such that the interior looks like the interior from an earlier  $T_{10}$ .

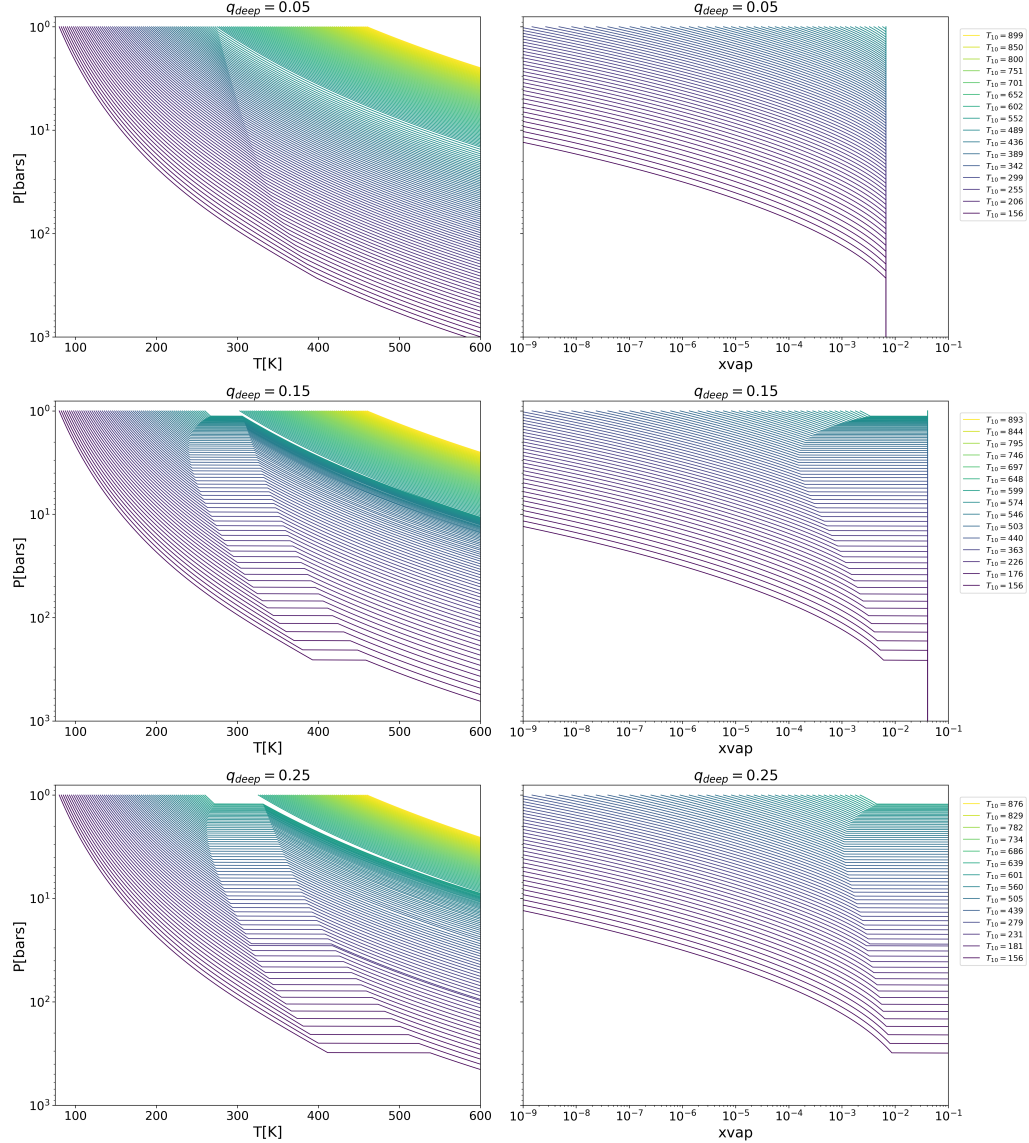


**Figure 3.3:** These plots were generated using our model Uranus. Again, from top to bottom row, we move from  $q_{\text{deep}} = 0.05$ , 0.15, and 0.25, respectively.  $T_{10}$ 's range from hotter (yellow) to cooler (purple), more recent temperatures. In the top row, no stable radiative zones are formed. The kink visible in the middle of the top left plot represents the transition from a moist to dry adiabat. Condensation occurs, but no stability is achieved. In rows two and three, stable radiative zones are formed, as indicated by the discontinuous temperature jumps moving left to right. The radiative zones form deeper in the interior as the planet cools. The plots in the second column show the vapor mole fraction with respect to pressure. The vapor mole fraction is constant within the radiative zone and reaches its deep water concentration value at the bottom of the radiative zone.

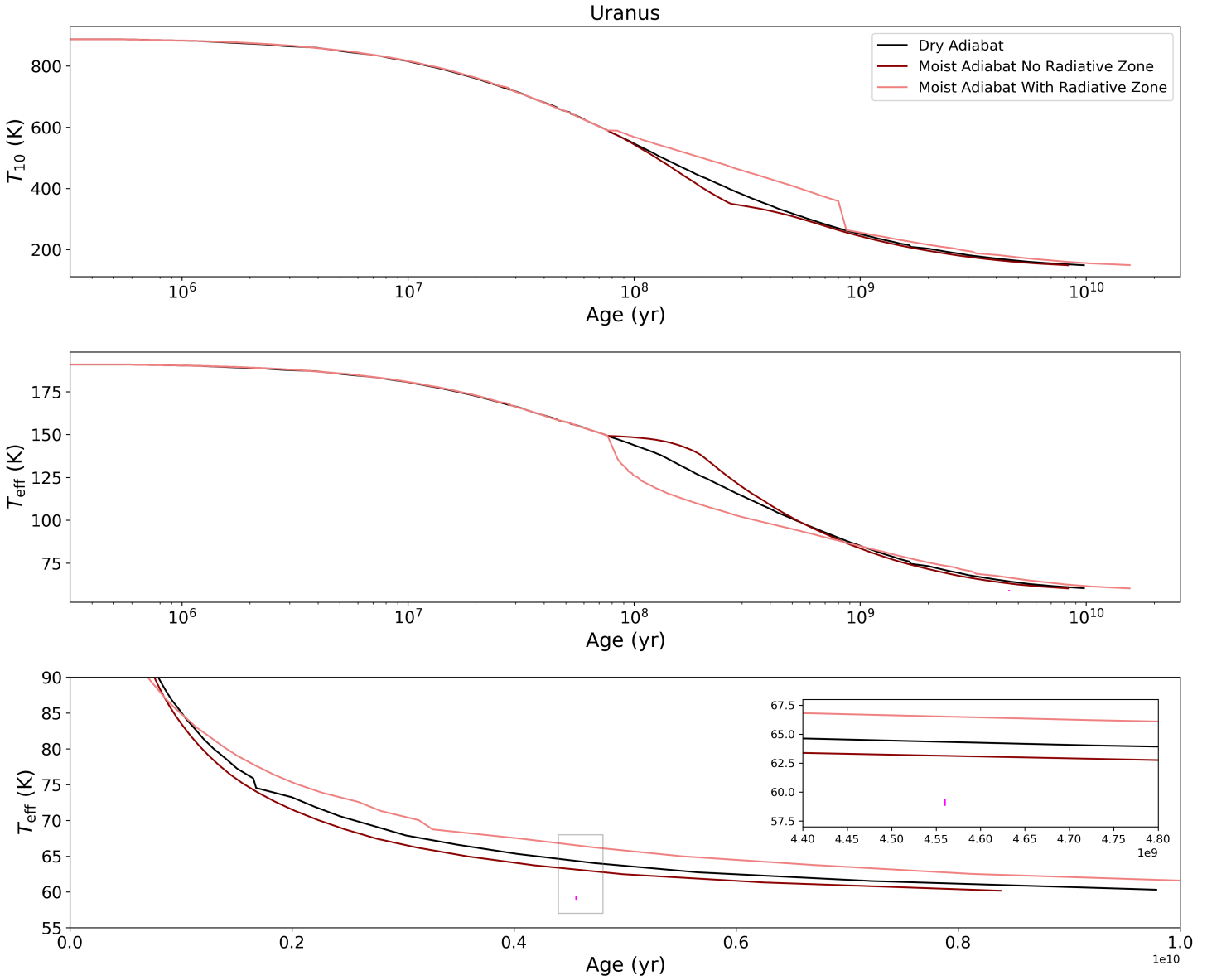


**Figure 3.4:** The black line represents the thermal evolution for a dry adiabat. The dark red line represents the thermal evolution for a moist adiabat that does not allow for the formation of a stable radiative layer. The light red line represents the thermal evolution of a moist adiabat that does allow for the formation of a stable radiative zone. The fuchsia dot on the lower plot represent the currently observed effective temperature of Uranus [include temp], plus or minus [include temp error].

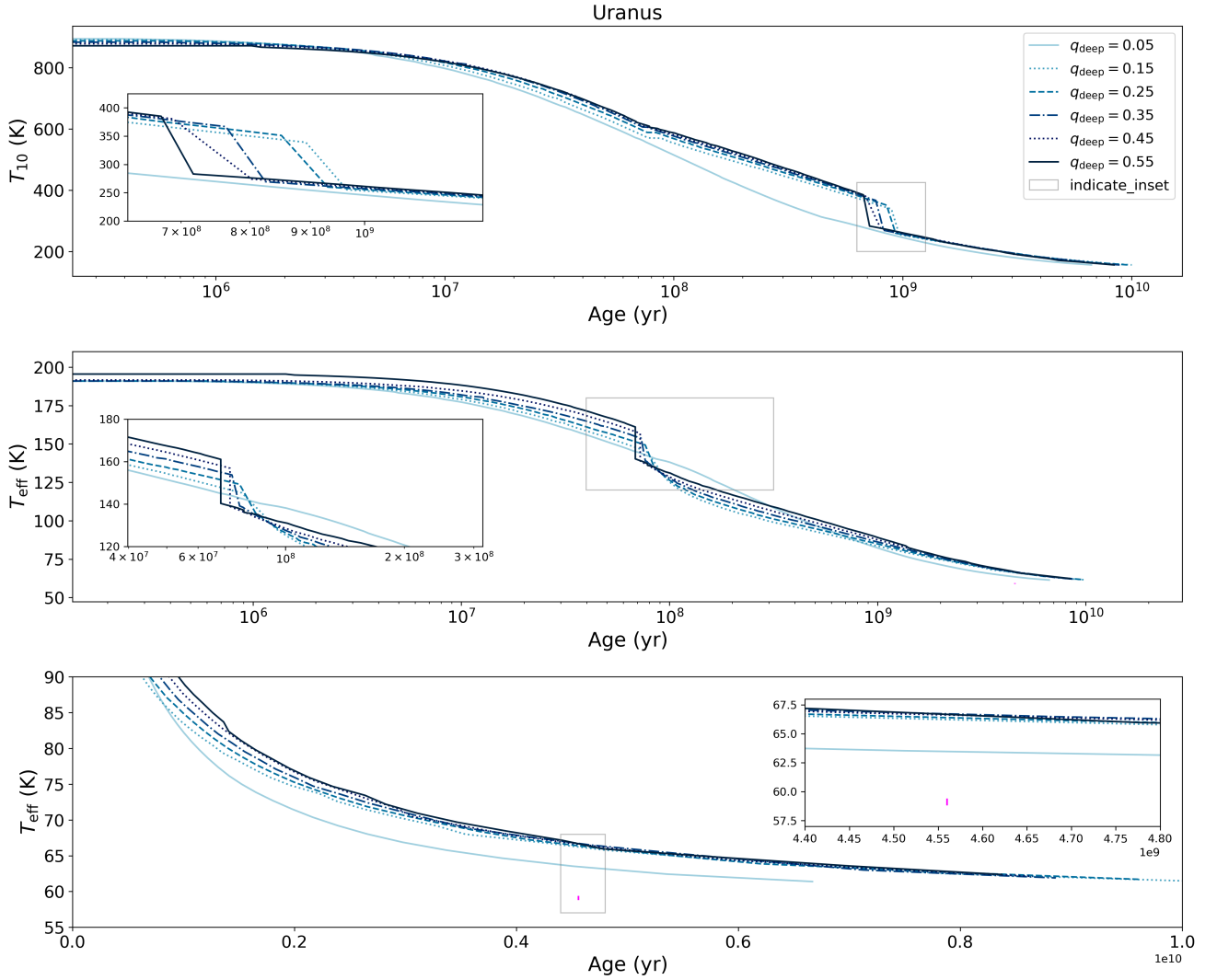


**Figure 3.5:** The curves in these plots represent thermal evolution tracks for different values of  $q_{\text{deep}}$ . Dark blue is the largest concentration of water vapor, at  $q_{\text{deep}} = 0.55$  and the light blue line is the least concentration of water vapor at  $q_{\text{deep}} = 0.05$ . For  $q_{\text{deep}} = 0.05$ , there is no onset of condensation-inhibited convection and no rapid cooling episode. For larger values of  $q_{\text{deep}}$  there is a rapid cooling episode for  $T_{\text{eff}}$  at around  $10^8$  Gyr. Similarly, a rapid cooling episode is visible deeper down in the interior as seen in the  $T_{10}$  curves at around  $10^9$  Gyr.

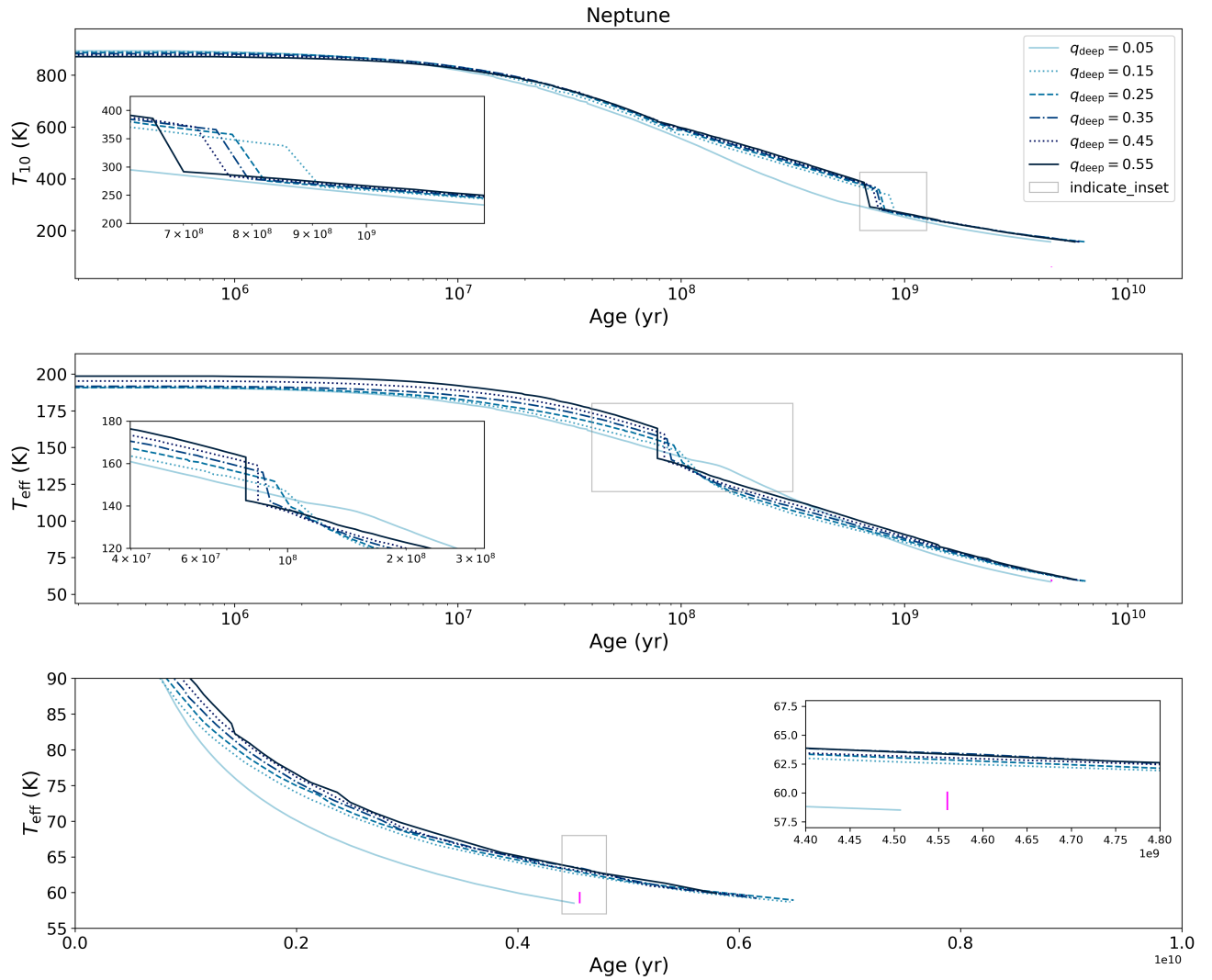


**Figure 3.6:** Similar to the Uranus plots, these curves represent cooling tracks for  $q_{\text{deep}}$ 's ranging from 0.05 to 0.55. Similar to Uranus, the rapid cooling episodes for  $T_{\text{eff}}$  and  $T_{10}$  occur at  $10^8$  Gyr and  $10^9$  Gyr, respectively. The vertical fuchsia line in the bottom plot indicates the current observed effective temperature of Neptune [include temp], plus or minus [include temp error]

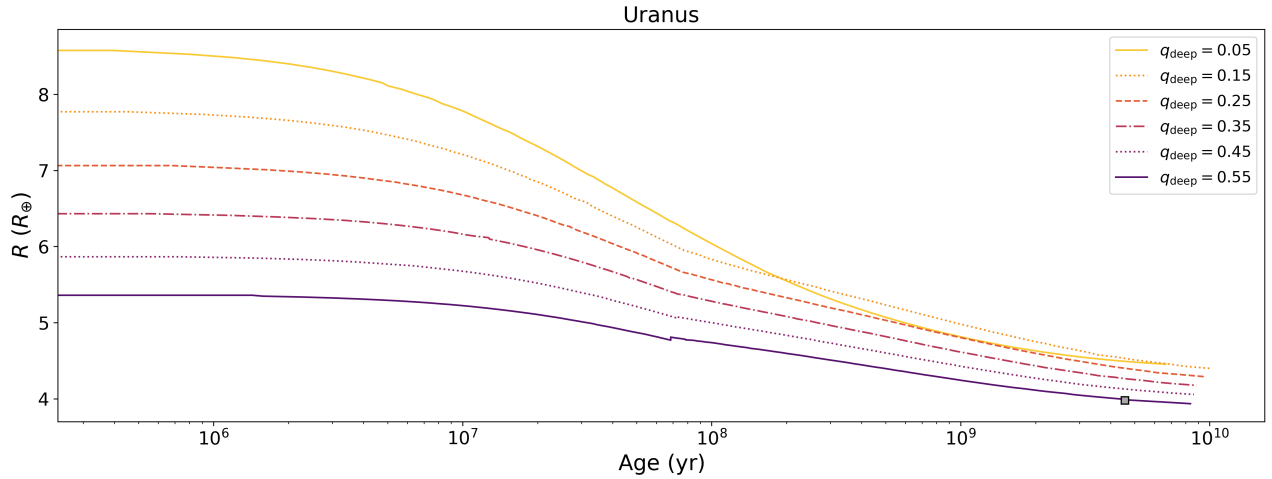


**Figure 3.7:** This thermal evolution plot shows the impact of different deep water concentration on the radius as the planet cools. The gray square represents the current observed radius.

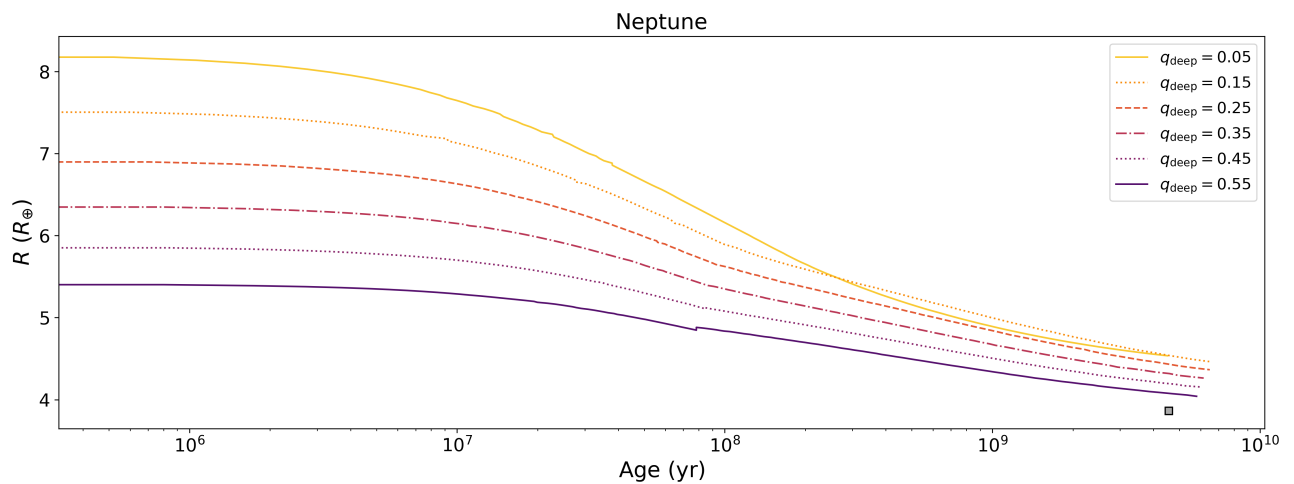


**Figure 3.8:** [Combine this plot with the above and have one caption.]

**4**

## Discussion and Conclusions

[I wrote this just before sending. I'm sure I'll want to make changes when i re-read in the morning] We set out to investigate the impact of water condensation zones on the thermal evolution of our solar system ice giants. It has been speculated that such thermal boundary layers could act as an imperfect insulator, trapping heat below and allowing the envelope above the boundary layer to cool more rapidly (Nettelmann et al., 2016)(Friedson & Gonzales, 2017)(Leconte et al., 2017)(M. Podolak, 1991)(L. Scheibe, 2019). It seems plausible that interiors containing these thermal boundary layers could explain the problem with Uranus appearing to have no intrinsic temperature. Our findings are inconclusive. We do find that incorporating a moist adiabat into our interior structure model does result in a cooler planet than would otherwise be seen with a purely dry model. However, when we add stable radiative zones to the interior, we do find in the planet's past a period of rapid cooling that results in a cooler effective temperature at around  $10^8$  Gyr, the planet eventually becomes warmer at present time than predicted by dry or simple moist adiabatic models. Reality is certainly more complex than the assumptions upon which our model is

based. It is quite possible that reality resembles something in between the binary choice of a moist adiabat with or without thermal boundary layers(Guillot, 2020). Our assumption of a stable shell of water condensation assumes that there are no other dynamics at play, such as upwelling or entrainment pressure (Friedson & Gonzales, 2017) eroding and punching holes in the stable radiative zone. Such scenarios could allow for more mixing of the warm gases below and above the condensation zone. We also considered only one condensate,  $H_2O$ . It would be worth considering  $NH_3$  and  $CH_4$ , and analyzing the impact of multiple stratified layers on the cooling of the planet over time.

# Bibliography

- Demarcus, W. C. (1958). The constitution of Jupiter and Saturn. *Astronomical Journal*, 63, 2.
- Fortney, J. J. & Hubbard, W. B. (2003). Phase separation in giant planets: inhomogeneous evolution of Saturn. *Icarus*, 164(1), 228–243.
- Fortney, J. J., Ikoma, M., Nettelmann, N., Guillot, T., & Marley, M. S. (2011). Self-consistent Model Atmospheres and the Cooling of the Solar System’s Giant Planets. *Astrophysical Journal*, 729(1), 32.
- Friedson, A. J. & Gonzales, E. J. (2017). Inhibition of ordinary and diffusive convection in the water condensation zone of the ice giants and implications for their thermal evolution. *Icarus*, 297, 160–178.
- Graboske, H. C., J., Pollack, J. B., Grossman, A. S., & Olness, R. J. (1975). The structure and evolution of Jupiter: the fluid contraction stage. *Astrophysical Journal*, 199, 265–281.
- Guillot, T. (1995). Condensation of Methane, Ammonia, and Water and the Inhibition of Convection in Giant Planets. *Science*, 269(5231), 1697–1699.

- Guillot, T. (2020). Uranus and Neptune are key to understand planets with hydrogen atmospheres. In *European Planetary Science Congress* (pp. EPSC2020–514).
- Hubbard, W. B. (1968). Thermal structure of Jupiter. *Astrophysical Journal*, 152, 745–754.
- Hubbard, W. B. (1977). The Jovian Surface Condition and Cooling Rate. *Icarus*, 30(2), 305–310.
- Hubbard, W. B. (1978). Comparative thermal evolution of Uranus and Neptune. *Icarus*, 35(2), 177–181.
- L. Scheibe, N Nettelmann, R. R. (2019). Thermal evolution of uranus and neptune: Adiabatic models. *Astronomy and Astrophysics*, A70, 632.
- Lavega, A. S. (2011). *Introduction to Planetary Atmospheres*. Taylor and Francis Group, LLC.
- Leconte, J. & Chabrier, G. (2013). Layered convection as the origin of Saturn's luminosity anomaly. *Nature Geoscience*, 6(5), 347–350.
- Leconte, J., Selsis, F., Hersant, F., & Guillot, T. (2017). Condensation-inhibited convection in hydrogen-rich atmospheres . Stability against double-diffusive processes and thermal profiles for Jupiter, Saturn, Uranus, and Neptune. *Astronomy and Astrophysics*, 598, A98.
- Low, F. J. (1966). Observations of Venus, Jupiter, and Saturn at  $\lambda 20 \mu$ . *Astronomical Journal*, 71, 391.
- M. Podolak, W.B. Hubbard, D. S. (1991). Models of uranus' interior and magnetic field. *Uranus*, Editors: J.T. Bergstrahl, E.D. Miner, M. Shapely Matthews, (pp.29).

Mankovich, C. & Fortney, J. J. (2019). Evidence for a Dichotomy in the Interior Structures of Jupiter and Saturn from Helium Phase Separation. In *AGU Fall Meeting Abstracts*, volume 2019 (pp. P24B–02).

Nettelmann, N., Wang, K., Fortney, J. J., Hamel, S., Yellamilli, S., Bethkenhagen, M., & Redmer, R. (2016). Uranus evolution models with simple thermal boundary layers. *Icarus*, 275, 107–116.

Pearl, J. C. & Conrath, B. J. (1991). The albedo, effective temperature, and energy balance of Neptune, as determined from Voyager data. *Journal of Geophysical Research*, 96, 18921–18930.

R. Kippenhahn, A. Weigert, A. W. (2012). *Stellar Structure and Evolution*. Springer.

Robinson, T. (2016). The moist pseudo-adiabat for multiple condensing species.

S. Mazevert, A. Licari, G. C. & Potekhin, A. Y. (2019). Ab initio based equation of state of dense water for planetary and exoplanetary modeling. *Astronomy & Astrophysics*, A128, 621.

Seager, S. (2010). Exoplanet atmospheres.

Smoluchowski, R. (1967). Internal Structure and Energy Emission of Jupiter. *Nature*, 215(5102), 691–695.

W.B. Hubbard, D. S. (1995). The interior of neptune. *Neptune and Triton*, Editor: D.P. Kruikshank, (pp. 109).

Y. Miguel, T. G. & Fayon, L. (2018). Jupiter internal structure: the effect of different equations of state. *Astronomy & Astrophysics*, C2, 618.